ACS Medicinal Chemistry Letters

pubs.acs.org/acsmedchemlett Letter

BTZ-Derived Benzisothiazolinones with In Vitro Activity against *Mycobacterium tuberculosis*

Adrian Richter, Rüdiger W. Seidel, Richard Goddard, Tamira Eckhardt, Christoph Lehmann, Julia Dörner, Fabienne Siersleben, Theresia Sondermann, Lea Mann, Michael Patzer, Christian Jäger, Norbert Reiling, and Peter Imming*

Cite This: *ACS Med. Chem. Lett.* 2022, 13, 1302−1310 Read Online

ACCESS | Metrics & More | Article Recommendations | Supporting Information

ABSTRACT: 8-Nitro-1,3-benzothiazin-4-ones (BTZs) are known as potent antitubercular agents. BTZ043 as one of the most advanced compounds has reached clinical trials. The putative oxidation products of BTZ043, namely, the corresponding BTZ sulfoxide and sulfone, were reported in this journal (Tiwari et al. *ACS Med. Chem Lett.* **2015**, *6*, 128−133). The molecular structures were later revised to the constitutionally isomeric benzisothiazolone and its 1-oxide, respectively. Here, we report two BTZ043-derived benzisothiazolinones (BITs) with in vitro activity against mycobacteria. The constitutionally isomeric *O*-acyl benzisothiazol-3-ols, in contrast, show little or no antimycobacterial activity in vitro. The structures of the four compounds were investigated by X-ray crystallography and NMR spectroscopy. Molecular covalent docking of the new compounds to *Mycobacterium tuberculosis* decaprenylphosphoryl-β-d-ribose 2′-epimerase (DprE1) suggests that the active BITs exert antimycobacterial activity through inhibition of DprE1 like BTZs.

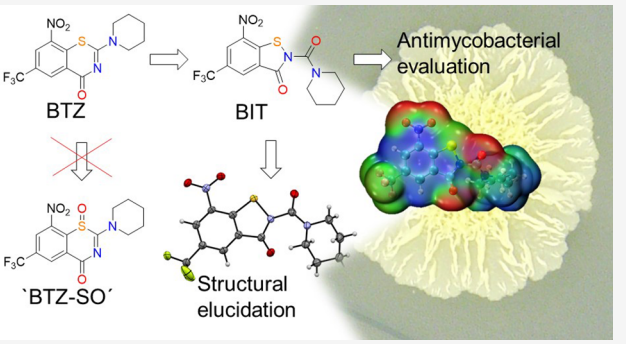

KEYWORDS: *benzisothiazolinone, BTZ043, crystal structure, antimycobacterial activity, DprE1, tuberculosis*

Tuberculosis (TB), the disease usually caused by *Mycobacterium tuberculosis*, globally continues to be the leading cause of death from a bacterial infectious agent.[1] According to the World Health Organization, a total of 1.5 million people died from and an estimated 9.9 million people fell ill with TB in 2020.[2] In particular, the increasing emergence of drug-resistant TB is a threat to public health.[3,4] Whereas about 85% of patients with drug-susceptible active TB can be successfully treated with a six-month regime of four first-line drugs,[2] treatment of drug-resistant TB in general takes longer, requires more expensive drugs that result in more side effects, and has lower success rates.[5,6] Drug discovery efforts are thus vital to combat drug-resistance and to reduce the duration, cost, and side effects of TB therapy through maintaining a copious anti-TB drug supply.[7−9]

8-Nitro-1,3-benzothiazin-4-ones (BTZs) have been identified as potent antitubercular agents.[10] The two most advanced compounds of this class, BTZ043 (Scheme 1) and macozinone (PBTZ169),[11] have progressed to clinical studies.[7] BTZs and several other electron-deficient nitroaromatic agents target the mycobacterial enzyme decaprenylphosphoryl-β-d-ribose 2′-epimerase (DprE1),[12−14] which is crucial for the biosynthesis of arabinogalactan, a major structural component of the mycobacterial cell wall. Upon binding to the active site of DprE1, the BTZ nitro group is reduced to a reactive nitroso group, which then forms a covalent semimercaptal with the thiol group of cysteine 387.[15] BTZs are thus mechanism-based inhibitors, which irreversibly inactivate the enzyme. For this mechanism of action, an electron-deficient warhead is essential. Besides the nitro group it was recently shown that 8-cyano BTZs also have antimycobacterial activity.[16] Efforts to modify the substituent at position 6 and the side chain at position 2 of the BTZ scaffold to improve physicochemical properties have been made.[17−20] Alteration of the BTZ core by means of scaffold simplification[21] and metabolically relevant chemical transformations of the scaffold have also been reported.[22,23]

In 2015, Tiwari et al. described the purported sulfoxide ("BTZ-SO") and sulfone ("BTZ-SO_2") of BTZ043 in this journal,[24] putatively obtained in very low yields by reaction of BTZ043 with the *m*-chloroperoxybenzoic acid (Scheme 1). The chemical structures of "BTZ-SO" and "BTZ-SO_2", as

Received: May 10, 2022
Accepted: July 15, 2022
Published: July 25, 2022

https://doi.org/10.1021/acsmedchemlett.2c00215
ACS Med. Chem. Lett. 2022, 13, 1302−1310

Scheme 1. Reaction of BTZs 1a and 1b (BTZ043) with *m*-Chloroperoxybenzoic Acid (*m*CPBA): Putative Chemical Structures "BTZ-SO" and "BTZ-SO_2" Assigned by Tiwari et al.[24] and Corresponding Revised Chemical Structures Reported by Eckhardt et al.[25]

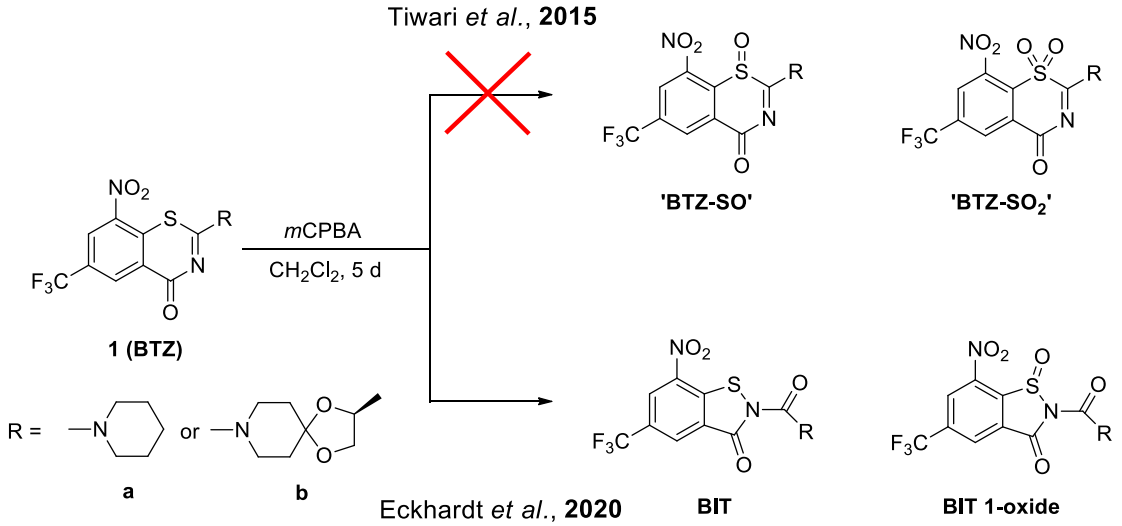

Scheme 2. Syntheses of *N*-Acyl BITs 4a and 4b and *O*-Acyl Benzisothiazolols 5a and 5b[a]

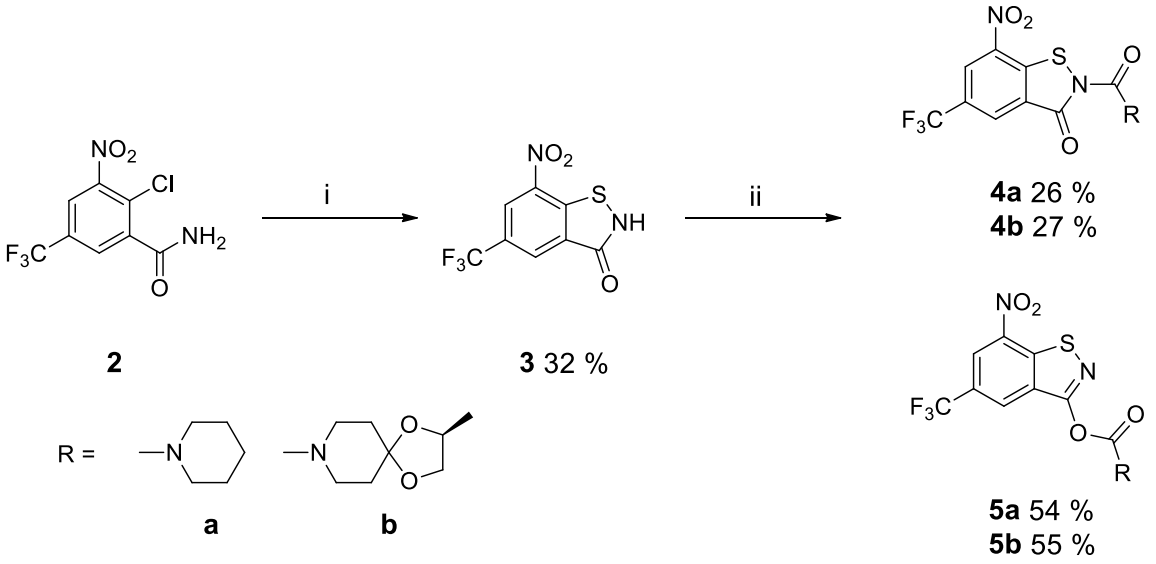

[a]Reagents and conditions: (i) CuI, 1,10-phenanthroline, sulfur, K_2CO_3, DMF, 110 °C, overnight; (ii) piperidine-1-carbonyl chloride (a) or (*S*)-2-methyl-1,4-dioxa-8-azaspiro[4.5]decane-8-carbonyl chloride (b), pyridine, CH_2Cl_2, rt, 24 h.

depicted in Scheme 1, were assigned on the basis of ^{1}H NMR spectroscopy and ESI mass spectrometry.

Unexpected upfield shifts of the two aromatic ^{1}H NMR signals, as compared with the parent BTZ043, were attributed to the influence of the lone pair at the sulfur atom and loss of aromaticity due to puckering of the thiazinone ring, as observed in AM1 computed molecular structures of the anticipated "BTZ-SO" and "BTZ-SO_2". Recently, X-ray crystallography revealed that the supposed BTZ sulfones resulting from treatment of BTZs **1a** and **1b** with *m*-chloroperoxybenzoic acid are in fact the corresponding benzisothiazolinone (BIT) 1-oxides (Scheme 1), which represent constitutional isomers.[25] Crystallographic evidence for the unintended BIT 1-oxide formation, retrosynthesis of a BIT and revisiting the ^{1}H NMR data eventually led to the revision of the chemical structures as depicted in Scheme 1 by Eckhardt et al. in 2020. In vitro activity data included in the previous reports revealed that the BITs exhibit comparable or better in vitro activity against *M. tuberculosis* and *Mycobacterium aurum* than the corresponding BTZs **1a** and **1b**.[25] This prompted us to further investigate these compounds. In this contribution, we report on the synthesis, structural characterization, and in vitro and in silico antimycobacterial evaluation of two BITs and their *O*-acyl benzisothiazol-3-ol constitutional isomers. The chemistry used to prepare the compounds studied is outlined in Scheme 2. *N*-Acyl BITs **4** and *O*-acyl benzisothiazolols **5** were synthesized in two steps from 2-chloro-5-trifluoromethyl-3-nitrobenzamide[26] (**2**). In the first step, BIT **3** was synthesized from **2** by a copper-mediated sulfur−nitrogen coupling reaction.[27] In the second step, **3** was reacted with piperidine-1-carbonyl chloride (for **4a** and **5a**) or (*S*)-2-methyl-1,4-dioxa-8-azaspiro[4.5]decane-8-carbonyl

https://doi.org/10.1021/acsmedchemlett.2c00215
ACS Med. Chem. Lett. 2022, 13, 1302−1310

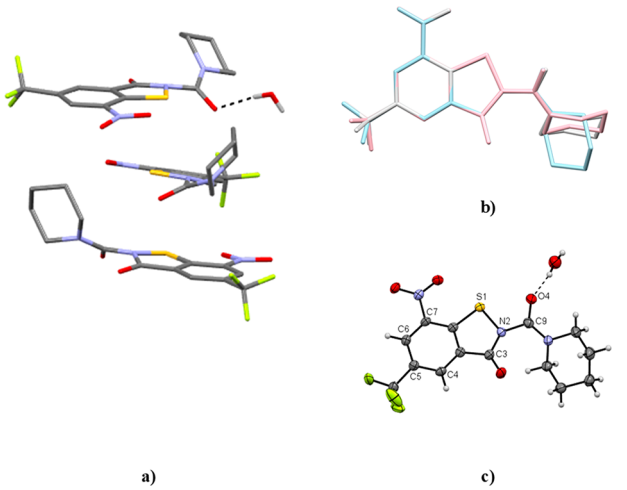

Figure 1. Crystal structure of **4a**·0.25 H_2O. (a) Asymmetric unit. Carbon-bound hydrogen atoms are omitted for clarity. (b) Structure overlay (benzene rings) of the three crystallographically unique molecules (pink, blue, gray). (c) Displacement ellipsoid plot (50% probability) of molecule 1. Rotational disorder of the trifluoromethyl group and positional disorder of a water hydrogen atom are not shown for clarity. Color scheme: C, gray; H, white; N, blue; O, red; S, yellow.

chloride[23,28] (for **4b** and **5b**)[29,30] to obtain **4** and **5**. Using pyridine as a base instead of triethylamine significantly improved the yield in the latter step. Compounds **4a** and **5a** as well as **4b** and **5b** represent constitutional isomers, which were separated by flash chromatography in both cases. The benzisothiazol-3-ol system in **5a** and **5b** represents a tautomeric form of the BIT system in **4a** and **4b**. Concomitant *O*-acylation benzisothiazol-3-ol of the tautomer, which is expected to be less stable than the BIT form, affords isolable *O*-acyl derivatives **5**. The ratio of **4** to **5** was around 1:2 in both cases. Higher electron density and better steric accessibility of the oxygen atom of the isothiazol-3-ol form compared with the

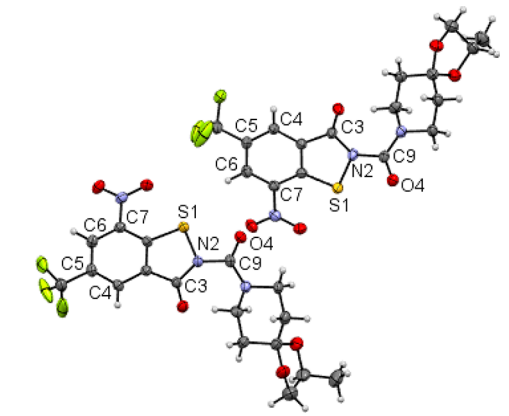

Figure 3. Asymmetric unit of the crystal structure of **4b**. Displacement ellipsoid plots are drawn at the 50% probability level. Rotational disorder of the trifluoromethyl groups is omitted for clarity. Color scheme: C, gray; H, white; N, blue; O, red; S, yellow.

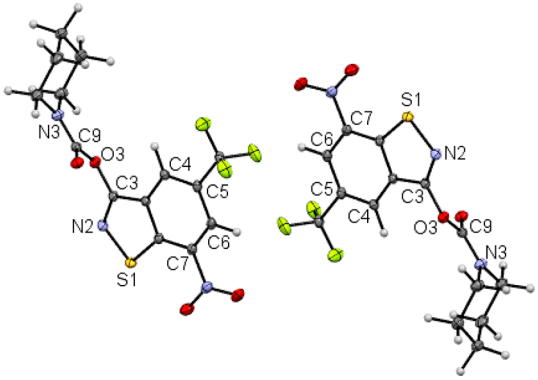

Figure 4. Section of the crystal structure of **5a**, showing two molecules related by a crystallographic inversion center. Displacement ellipsoids are drawn at the 50% probability level. The crystal structure was refined with aspherical scattering factors using NoSpherA2.[38] Color scheme: C, gray; H, white; N, blue; O, red; S, yellow.

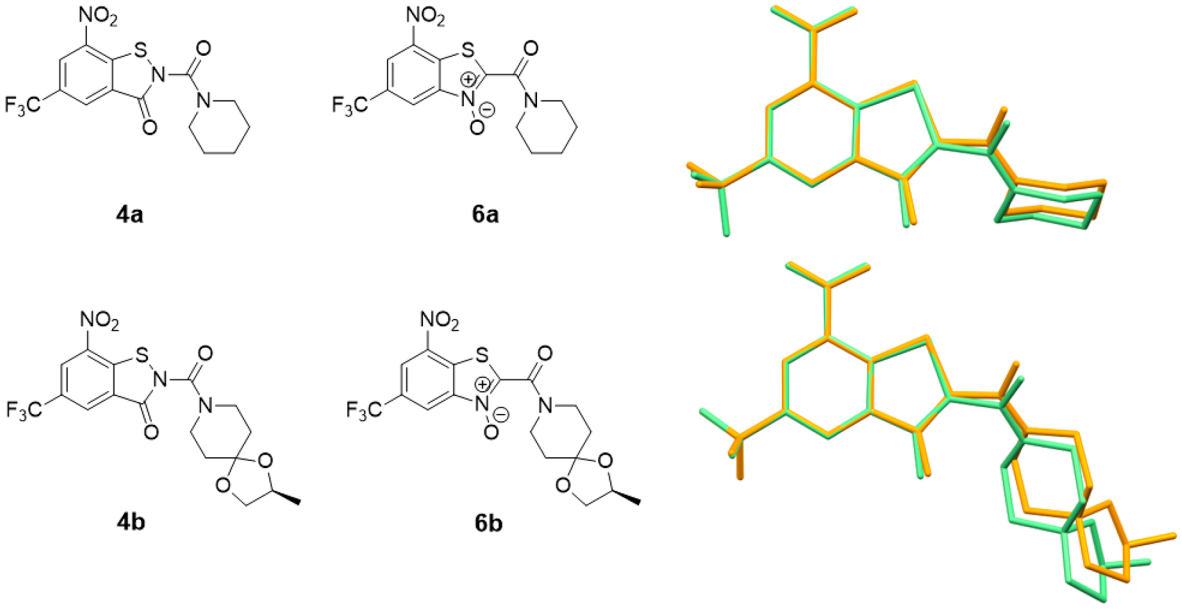

Figure 2. Chemical diagrams and structure overlay (benzene rings) of DFT-optimized molecular structures of **4a** and **4b** (orange) and the BTO constitutional isomers **6a**[32] and **6b** (green).[33] Hydrogen atoms are omitted for clarity.

https://doi.org/10.1021/acsmedchemlett.2c00215
ACS Med. Chem. Lett. 2022, 13, 1302−1310

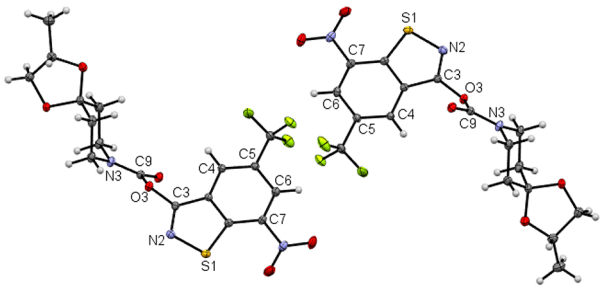

Figure 5. Asymmetric unit of the crystal structure of **5b**. Displacement ellipsoids are drawn at the 50% probability level. Color scheme: C, gray; H, white; N, blue; O, red; S, yellow.

isothiazol-3-one nitrogen atom likely explain the observed regioselectivity.

The structures of the reaction products **4a** and **4b** as well as isomeric **5a** and **5b** were unambiguously assigned by X-ray crystallography. Compound **4a** crystallized as a 0.25 hydrate with three crystallographically unique molecules.[31] As shown in Figure 1a, the three distinct molecules all adopt a *Z* conformation about the C_{acyl}–$N2_{BIT}$ bond. The appended piperidine ring adopts a chair conformation in each case (Figure 1b).

Table 1. In Vitro Activity (MIC_{90} in μM) of 4a, 4b, 5a, and 5b and the Two Reference BTZs 1a and 1b against *M. smegmatis* mc^2 155, *M. aurum* DSM 43999 and *M. tuberculosis* H37Rv

	M. smegmatis mc^2 155[a]	*M. aurum* DSM 43999[b]	*M. tuberculosis* H37Rv[b]
1a	6.25	25−12.5	>4.0
1b (BTZ043)	0.025	0.008	<0.06
4a	0.20	0.10	1.0
4b	0.32	0.25−0.13	0.5
5a	>100	>100	>32
5b	>100	>100	>32

[a]7H9 medium supplemented with ADS. [b]7H9 medium supplemented with OADC.

The solvate water forms a hydrogen bond to the piperidinoyl oxygen atom of molecule 1 (Figure 1c). Figure 2 depicts overlay diagrams of DFT-calculated molecular structures of **4a** and **4b** and the corresponding constitutionally isomeric benzothiazole *N*-oxides (BTOs, **6**), potent antimycobacterial agents described previously in the literature (vide infra),[32,33] which reveals that the molecules are isosteric.

Compound **4b** crystallizes with two molecules in the asymmetric unit (Figure 3).[34] Like in **4a**, the conformation

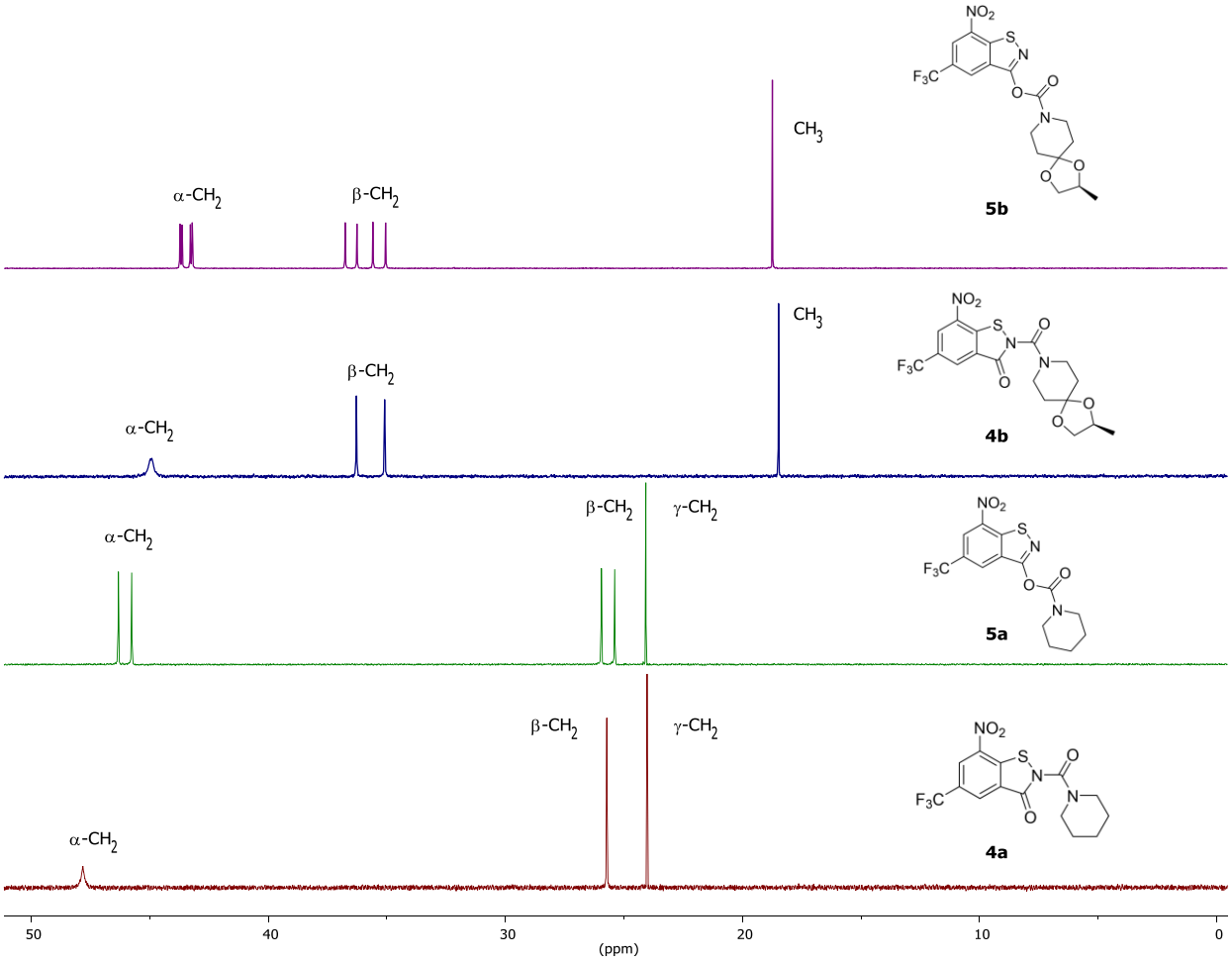

Figure 6. Aliphatic region of the ^{13}C NMR spectra of **4a**, **5a**, **4b**, and **5b** in $CDCl_3$ at room temperature (the full spectra are shown in the Supporting Information).

https://doi.org/10.1021/acsmedchemlett.2c00215
ACS Med. Chem. Lett. 2022, 13, 1302−1310

Table 2. Physicochemical Properties of 4a, 4b, 5a, and 5b, the Two Reference BTZs 1a and 1b, and the precursor 3

	solubility (μM)[a]	c log P[b]
1a	85	3.39
1b (BTZ043)	74	2.45
3	444	1.23
4a	92	4.14
4b	103	3.47
5a	60	3.75
5b	39	2.81

[a]Determined by nephelometry in PBS (pH 7.4) with 2% (v/v) DMSO.[44] [b]Calculated with *Chem3D Ultra* version 20.1.1.125.

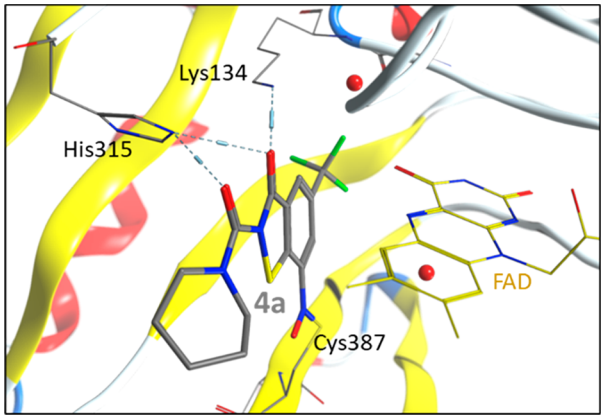

Figure 7. Highest ranked molecular covalent docking solution of **4a** to *M. tuberculosis* DprE1.

about the C_{acyl}–$N2_{BIT}$ bond is *Z* in both unique molecules. The two crystallographically distinct molecules are thus diastereomeric conformers. Such was also encountered in the crystal structure of **1b** (BTZ043).[35]

Figures 4 and 5 depict the molecular structures of **5a** and **5b**, respectively, in the crystal.[36,37] The C3–N2 bond length of the benzothiazole heterocyclic system of 1.298(1) Å is significantly shorter by ca. 0.4 Å than that in **4a** and **4b**, consistent with C=N double bond character in **5a** and **5b**. The opposite enantiomeric conformer is also present in the centrosymmetric crystal structure. As for **1b**[35] and **4b**, the crystal structure of **5b** comprises two crystallographically unique diastereomeric conformers.

Compounds **4** and **5** were also structurally characterized by ^{1}H and ^{13}C NMR spectroscopy in solution at room temperature (see the Supporting Information). Figure 6 shows the aliphatic regions of the ^{13}C NMR spectra in $CDCl_3$, which exhibit the most marked differences for the compounds studied. The resonance signals in the aliphatic regions were assigned based on chemical shifts. With three signals, **4a** shows the simplest spectrum in this region. The signals are assigned to the piperidine methylene groups. The occurrence of one set of signals for the α- and β-methylene groups indicates that rotation about the urea $C_{carbonyl}$–$N_{piperidine}$ bond is fast. The same was observed for BTZ **1a**.[20] In contrast, two signals are encountered for each of the α- and β-methylene groups in the spectrum of **5a**, which can the explained by restricted rotation of the piperidine ring around the $C_{carbonyl}$–$N_{piperidine}$ bond. For **4b** and **5b**, the most upfield shifted signal is assigned to the methyl group of the methyldioxolan moiety. For **4b**, two signals appear for the piperidine β-methylene groups, whereas the α-methylene carbon atoms are virtually isochronous, suggesting that there is no restricted rotation of the side chain around the $C_{carbonyl}$–$N_{piperidine}$ bond. For BTZ **1b**, variable-temperature ^{13}C NMR spectroscopy revealed a coalescence temperature T_c of 301 ± 1 K and a Gibbs free energy $\Delta G^{\ddagger}$ of 14.6 ± 1 kcal mol^{-1} for this process.[35] The ^{13}C NMR spectrum of **5b** displays four discrete signals for each of the α- and β-piperidine methylene groups, which can be ascribed to diastereomeric conformers, as revealed by X-ray crystallography (Figure 5), resulting from restricted rotation of the side chain around both the carbamate $C_{carbonyl}$–$N_{piperidine}$ and C_{BIT}–O_{BIT} bonds. Restricted rotation around the C_{BIT}–O_{BIT} bond in **5a** due to steric clashes between the carbamate group and benzisothiazolol moiety should result in stable enantiomeric conformers, which cannot be distinguished in the NMR spectrum. As shown in Figure 4, both enantiomeric conformers of **5a** are present in the solid state.

Antimycobacterial activities of **4a**, **4b**, **5a**, and **5b** and BTZs **1a** and **1b** as reference compounds were determined in vitro against *Mycobacterium smegmatis*, *M. aurum*, and *M. tuberculosis* (Table 1). *M. smegmatis* and *M. tuberculosis* are susceptible to irreversible inhibition of DprE1 through BTZs,[10,39] because of the presence of a cysteine residue in the active site (vide supra). *M. smegmatis* is a fast-growing mycobacterium, generally considered nonpathogenic, and a useful model organism for *M. tuberculosis*.[40] We found that the *N*-acyl BITs **4a** and **4b** with the side chain appended to the BIT nitrogen atom exert activity against the three mycobacterial strains. Interestingly, **4a** is more active than BTZ **1a** bearing the same piperidine side chain. A similar trend, however, is not observed for **4b** and the corresponding BTZ **1b**. The in vitro activity of **4b** bearing the BTZ043-like side chain does not reach that of the **1b** but is similar to that of **4a**. The MIC values against the three mycobacterial strains are still some orders of magnitude higher for **4b** than for **1b**. The isomeric *O*-acyl benzisothiazol-3-ol derivatives **5a** and **5b** do not inhibit mycobacterial growth up to the concentrations tested. We propose that the carbamate group attached to the BIT oxygen atom (O3) and resulting altered hydrogen bond preferences account for the inactivity of **5a** and **5b** (vide infra). The BIT precursor **3**, lacking a side chain, was tested in vitro against *M. smegmatis* and found to be inactive (MIC_{90} > 100 μM) as expected. The in vitro test results for **3**, **5a**, and **5b** confirm that not only an electron-deficient nitroaromatic warhead but also the nature and spatial orientation of the side chain are critical for efficient mechanism-based mycobacterial growth inhibition. Kinetic solubilities of the compounds studied in PBS are essentially comparable with each other and with the two reference BTZs, and the c log *P* values are lower for the compounds bearing the BTZ043-like spiro ketal side chain than for those with an appended piperidine ring (Table 2). The c log *P* values of the active compounds **4a** and **4b** are higher than those of the corresponding inactive constitutional isomers **5a** and **5b** but do not exceed a value of 5, which is desirable for drug-like compounds.[41]

These results raise the question of how the antimycobacterial properties of **4a** and **4b** compare with those of the structurally most related compounds. As reported previously, **4a** and **4b** exhibited higher in vitro activity against *M. tuberculosis* and *M. aurum* than the corresponding BIT 1-oxides.[25] For the corresponding isosteric BTO constitutional isomers (vide supra), in vitro activity data against *M. tuberculosis* H37Rv can be found in the literature: 0.25 μg

https://doi.org/10.1021/acsmedchemlett.2c00215
ACS Med. Chem. Lett. 2022, 13, 1302–1310

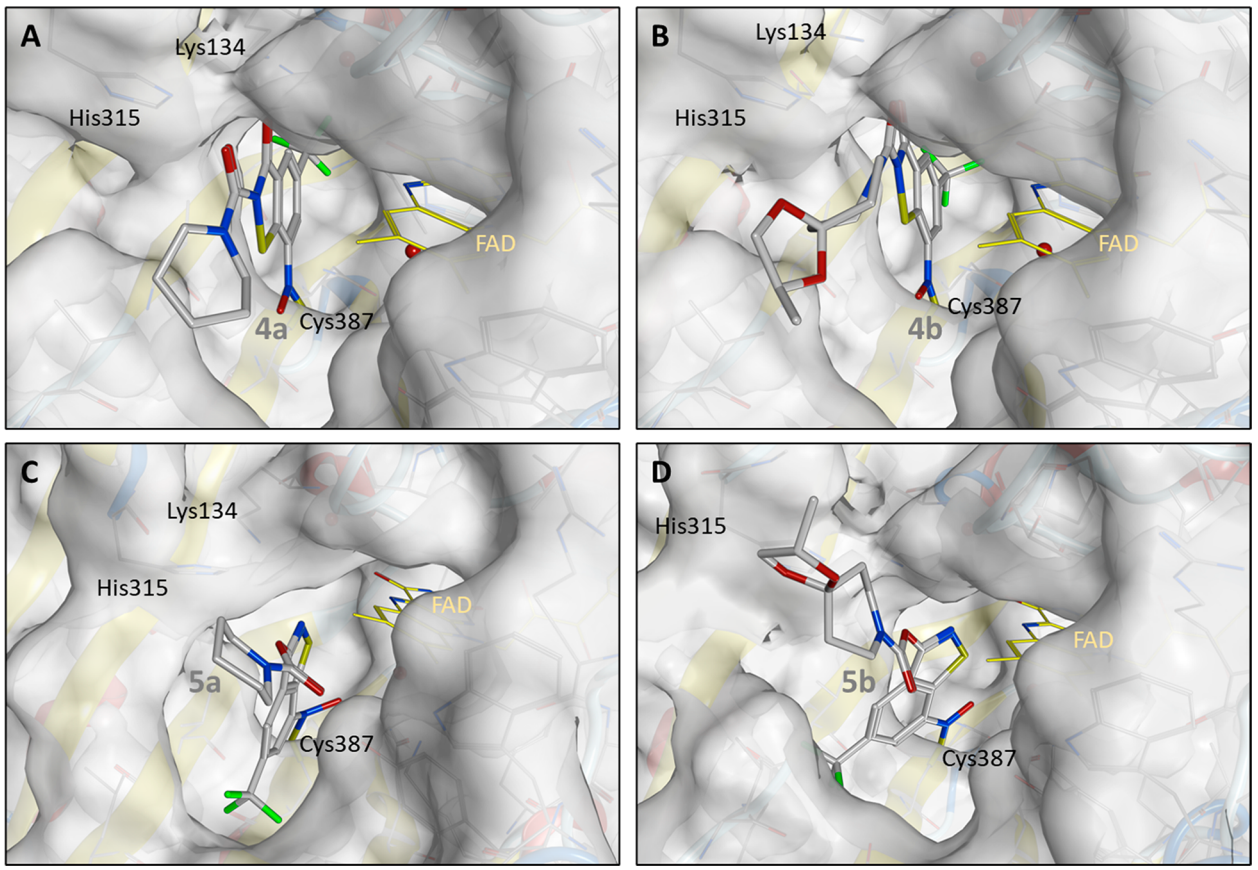

Figure 8. Highest ranked molecular docking solutions for (A) **4a**, (B) **4b**, (C) **5a**, and (D) **5b** (docked to 6HEZ.B; flexible side chains for Lys134, Trp230, Val365, Leu363, Lys418; toggled water molecules; solution number as in Table S2).

mL^{-1} (0.67 μM) for **6a**[32] (medium unknown) and 0.24 μM (7H12 medium) and 0.23 μM (GAS medium) for **6b**.[33] Thus, **4a**/**4b** and **6a**/**6b** exhibit comparable in vitro activities against *M. tuberculosis*. Comparing the molecular electrostatic potential (MEP) mapped onto the van der Waals surface for **4a**/**4b** versus **6a**/**6b** reveals a striking similarity of the isosteric molecules (see the Supporting Information). The comparable antimycobacterial properties are consistent with these findings. The authors of **6a** also reported the crystal structure of a related BTO (bearing a different side chain) in complex with *M. tuberculosis* DprE1 (PDB ID: 4PFA),[32] which revealed a semimercaptal adduct formed between the nitroso form of the ligand and the Cys387 residue like for BTZs (vide supra). The authors of **6b** proved by metabolic labeling of *M. tuberculosis* DprE1 and in vitro testing against *M. aurum* that the target for this BTO compound is DprE1, based on the assumption that *M. aurum* lacks a cysteine residue in the DprE1 active site[42] [U. Möllmann, M. Miller, personal communication: In ref 33, the *M. aurum* strain SB66 from the collection of the Leibniz Institute for Natural Product Research and Infection Biology – Hans Knöll Institute – (HKI, Jena, Germany) was used.].[33]

As shown in Table 2 below, the active BIT derivatives **4a** and **4b** have a similar low solubility as lead compound BTZ043 (≤100 μM), whereas the c log *P* values are slightly higher.

In the present work, we observed that BITs **4a**/**4b** and BTZs **1a**/**1b** inhibit growth of *M. aurum* DSM 43999, which is consistent with our previously reported results for **1a** and **4a**.[25] In their report on the purported "BTZ-SO",[24] whose structure we revised to **4b** (vide supra), Tiwari et al. described growth inhibition of *M. aurum* SB66 by "BTZ-SO", but not by **1b** (BTZ043). This also could be due to DprE1 sequence differences between the two *M. aurum* strains. We should also note that BITs are known to have various molecular targets in microorganisms.[43]

Molecular covalent docking of the newly synthesized compounds **4a**, **4b**, **5a**, and **5b** to *M. tuberculosis* DprE1 was performed to gain insight into possible binding modes. The docking pose of **1b** corresponds to the orientation encountered in the crystal structure in complex with the *M. tuberculosis* DprE1 (PDB ID: 6HEZ)[15] (see the Supporting Information). The binding mode of the active compounds **4a** and **4b** shows a comparable orientation in the active site for all highly evaluated docking poses. Therefore, it is reasonable to assume that the secondary interactions can be formed similarly to **1b**. In comparison to **4b**, the position of **4a** changes slightly. This can be attributed to the fact that the bridged hydrogen bond, formed to FAD, which is apparent in the crystal structure of **1b** in complex with DprE1 (chain B), is observed in docked solutions of **4b** but not **4a**. Stabilizing effects are, however, noticeable via hydrogen bonds to Lys134 and His315 for this compound. In particular, the possible formation of a hydrogen bond between the amino group of the Lys134 side chain and O3 of **4a** is striking (Figure 7).

The results for the inactive **5a** and **5b** are quite different. For these molecules, none of the in silico methods could provide a placement similar to that described above. All docking solutions for **5a** and **5b** resulted in a pose of the molecules rotated by nearly 180°. This is likely due to the fundamental change in the molecular structure with regard to the linkage of the piperidinoyl side chain to the molecular scaffold via the

https://doi.org/10.1021/acsmedchemlett.2c00215
ACS Med. Chem. Lett. 2022, 13, 1302−1310

benzothiazole oxygen atom O3, which subsequently leads to steric hindrance in the DprE1 active site. In addition, the hydrogen bond observed in the crystal structure of **1b** in complex with DprE1 can no longer be formed. All these indications rationalize the inactivity of **5a** and **5b**, which is confirmed by the total fitness scores of active **4a** and **4b** and inactive **5a** and **5b** (Table S1). The highest ranked solutions are shown in Figure 8.

In summary, the *N*-acyl BITs **4** and *O*-acyl benzisothiazolols **5** were synthesized and their structures investigated by X-ray crystallography and NMR spectroscopy. The *N*-acyl BITs **4** exhibited only slightly poorer activity against *M. smegmatis* mc^2 155a, *M. aurum* DSM 43999b and *M. tuberculosis* H37Rv than **1b** (BTZ043) and significantly better activity than **1a**, whereas **5** showed little or no antimycobacterial activity. Notably, **4a** is more active by an order of magnitude than BTZ **1a** bearing the same piperidine side chain. The in vitro test results for the BIT precursor **3** lacking a side chain, **5a** and **5b** confirm that not only an electron-deficient nitroaromatic warhead but also the nature and spatial orientation of the side group are critical for efficient mechanism-based mycobacterial growth inhibition. The inability of **5** to inhibit *M. tuberculosis* DprE1 was rationalized using in silico docking experiments on **4** and **5**, which attributed this to the linkage of the piperidinoyl side chain to the molecular scaffold via the benzothiazole oxygen atom O3.

■ ASSOCIATED CONTENT

Supporting Information

The Supporting Information is available free of charge at https://pubs.acs.org/doi/10.1021/acsmedchemlett.2c00215.

Experimental and computational details along with characterizations of the compounds synthesized (PDF)

DFT-calculated structure of **4a** (XYZ)

DFT-calculated structure of **4b** (XYZ)

DFT-calculated structure of **5a** (XYZ)

DFT-calculated structure of **5b** (XYZ)

DFT-calculated structure of **6a** (XYZ)

DFT-calculated structure of **6b** (XYZ)

Accession Codes

CCDC 2171377−2171380 contain the supplementary crystallographic data for this paper. These data can be obtained free of charge from the Cambridge Crystallographic Data Centre via www.ccdc.cam.ac.uk/structures.

■ AUTHOR INFORMATION

Corresponding Author

Peter Imming − *Martin-Luther-Universität Halle-Wittenberg, 06120 Halle (Saale), Germany;* orcid.org/0000-0003-2178-3887; Email: peter.imming@pharmazie.uni-halle.de

Authors

Adrian Richter − *Martin-Luther-Universität Halle-Wittenberg, 06120 Halle (Saale), Germany;* orcid.org/0000-0002-0062-7896

Rüdiger W. Seidel − *Martin-Luther-Universität Halle-Wittenberg, 06120 Halle (Saale), Germany;* orcid.org/0000-0003-3438-4666

Richard Goddard − *Max-Planck-Institut für Kohlenforschung, 45470 Mülheim an der Ruhr, Germany;* orcid.org/0000-0003-0357-3173

Tamira Eckhardt − *Martin-Luther-Universität Halle-Wittenberg, 06120 Halle (Saale), Germany*

Christoph Lehmann − *Martin-Luther-Universität Halle-Wittenberg, 06120 Halle (Saale), Germany*

Julia Dörner − *Martin-Luther-Universität Halle-Wittenberg, 06120 Halle (Saale), Germany*

Fabienne Siersleben − *Martin-Luther-Universität Halle-Wittenberg, 06120 Halle (Saale), Germany*

Theresia Sondermann − *Martin-Luther-Universität Halle-Wittenberg, 06120 Halle (Saale), Germany*

Lea Mann − *Martin-Luther-Universität Halle-Wittenberg, 06120 Halle (Saale), Germany*

Michael Patzer − *Max-Planck-Institut für Kohlenforschung, 45470 Mülheim an der Ruhr, Germany*

Christian Jäger − *Fraunhofer-Institut für Zelltherapie und Immunologie, Außenstelle Molekulare Wirkstoffbiochemie und Therapieentwicklung, 06120 Halle (Saale), Germany;* orcid.org/0000-0002-2740-8386

Norbert Reiling − *Microbial Interface Biology, Research Center Borstel, Leibniz Lung Center, 23845 Borstel, Germany; German Center for Infection Research (DZIF), 23845 Borstel, Germany;* orcid.org/0000-0001-6673-4291

Complete contact information is available at: https://pubs.acs.org/10.1021/acsmedchemlett.2c00215

Author Contributions

The manuscript was written through contributions of all authors.

Funding

This work was funded by the Deutsche Forschungsgemeinschaft (DFG, German Research Foundation) - 432291016.

Notes

The authors declare no competing financial interest.

■ ACKNOWLEDGMENTS

Professor Christian W. Lehmann is gratefully acknowledged for providing access to the X-ray diffraction facility. We would to thank Heike Schucht and Elke Dreher for technical assistance with the X-ray intensity data collections, Dr. Christian Ihling and Antje Herbrich-Peters for recording the HRMS spectra and Julia Seiser for the nephelometric measurements. Thanks are due to Dr. Jens-Ulrich Rahfeld and Dr. Nadine Taudte for providing and maintaining the biosafety level 2 facility. We also thank Lisa Niwinski (Borstel) for her expert technical assistance with the *M. tuberculosis* growth analyses under biosafety level 3 conditions.

■ DEDICATION

Dedicated to Professor Bodo Dobner on the occasion of his 70th birthday.

■ ABBREVIATIONS

BTZ, 8-nitro-1,3-benzothiazin-4-one; BIT, benzisothiazolinone; BTO, benzothiazole *N*-oxides; DprE1, decaprenylphosphoryl-β-d-ribose 2′-epimerase; *m*CPBA, *m*-chloroperoxybenzoic acid; MEP, molecular electrostatic potential

■ REFERENCES

(1) Dartois, V. A.; Rubin, E. J., Anti-tuberculosis treatment strategies and drug development: challenges and priorities. *Nature Reviews Microbiology* **2022**, DOI: 10.1038/s41579-022-00731-y.

(2) *Global Tuberculosis Report*; World Health Organization: Geneva, Switzerland, 2021.
(3) Koch, A.; Cox, H.; Mizrahi, V. Drug-resistant tuberculosis: challenges and opportunities for diagnosis and treatment. *Current Opinion in Pharmacology* **2018**, *42*, 7−15.
(4) Shah, I.; Poojari, V.; Meshram, H. Multi-Drug Resistant and Extensively-Drug Resistant Tuberculosis. *The. Indian Journal of Pediatrics* **2020**, *87* (10), 833−839.
(5) Lange, C.; Chesov, D.; Heyckendorf, J.; Leung, C. C.; Udwadia, Z.; Dheda, K. Drug-resistant tuberculosis: An update on disease burden, diagnosis and treatment. *Respirology* **2018**, *23* (7), 656−673.
(6) Lange, C.; Dheda, K.; Chesov, D.; Mandalakas, A. M.; Udwadia, Z.; Horsburgh, C. R. Management of drug-resistant tuberculosis. *Lancet* **2019**, *394* (10202), 953−966.
(7) Shetye, G. S.; Franzblau, S. G.; Cho, S. New tuberculosis drug targets, their inhibitors, and potential therapeutic impact. *Translational Research* **2020**, *220*, 68−97.
(8) Chauhan, A.; Kumar, M.; Kumar, A.; Kanchan, K. Comprehensive review on mechanism of action, resistance and evolution of antimycobacterial drugs. *Life Sciences* **2021**, *274*, 119301.
(9) Sharma, A.; De Rosa, M.; Singla, N.; Singh, G.; Barnwal, R. P.; Pandey, A. Tuberculosis: An Overview of the Immunogenic Response, Disease Progression, and Medicinal Chemistry Efforts in the Last Decade toward the Development of Potential Drugs for Extensively Drug-Resistant Tuberculosis Strains. *J. Med. Chem.* **2021**, *64* (8), 4359−4395.
(10) Makarov, V.; Manina, G.; Mikusova, K.; Möllmann, U.; Ryabova, O.; Saint-Joanis, B.; Dhar, N.; Pasca, M. R.; Buroni, S.; Lucarelli, A. P.; Milano, A.; De Rossi, E.; Belanova, M.; Bobovska, A.; Dianiskova, P.; Kordulakova, J.; Sala, C.; Fullam, E.; Schneider, P.; McKinney, J. D.; Brodin, P.; Christophe, T.; Waddell, S.; Butcher, P.; Albrethsen, J.; Rosenkrands, I.; Brosch, R.; Nandi, V.; Bharath, S.; Gaonkar, S.; Shandil, R. K.; Balasubramanian, V.; Balganesh, T.; Tyagi, S.; Grosset, J.; Riccardi, G.; Cole, S. T. Benzothiazinones Kill *Mycobacterium tuberculosis* by Blocking Arabinan Synthesis. *Science* **2009**, *324* (5928), 801−804.
(11) Makarov, V.; Mikušová, K. Development of Macozinone for TB treatment: An Update. *Applied Sciences* **2020**, *10* (7), 2269.
(12) Gawad, J.; Bonde, C. Decaprenyl-phosphoryl-ribose 2′-epimerase (DprE1): challenging target for antitubercular drug discovery. *Chemistry Central Journal* **2018**, *12* (1), 72.
(13) Chikhale, R. V.; Barmade, M. A.; Murumkar, P. R.; Yadav, M. R. Overview of the Development of DprE1 Inhibitors for Combating the Menace of Tuberculosis. *J. Med. Chem.* **2018**, *61* (19), 8563−8593.
(14) Imran, M..; A.S., A.; Thabet, H. K..; Abida; Afroz Bakht, M.. Synthetic molecules as DprE1 inhibitors: A patent review. *Expert Opinion on Therapeutic Patents* **2021**, *31* (8), 759−772.
(15) Richter, A.; Rudolph, I.; Möllmann, U.; Voigt, K.; Chung, C.-w.; Singh, O. M. P.; Rees, M.; Mendoza-Losana, A.; Bates, R.; Ballell, L.; et al. Novel insight into the reaction of nitro, nitroso and hydroxylamino benzothiazinones and of benzoxacinones with Mycobacterium tuberculosis DprE1. *Sci. Rep.* **2018**, *8* (1), 13473.
(16) Zhang, G.; Sheng, L.; Hegde, P.; Li, Y.; Aldrich, C. C. 8-cyanobenzothiazinone analogs with potent antitubercular activity. *Med. Chem. Res.* **2021**, *30*, 449−458.
(17) Fan, D.; Wang, B.; Stelitano, G.; Savková, K.; Shi, R.; Huszár, S.; Han, Q.; Mikušová, K.; Chiarelli, L. R.; Lu, Y.; Qiao, C. Structural and Activity Relationships of 6-Sulfonyl-8-Nitrobenzothiazinones as Antitubercular Agents. *J. Med. Chem.* **2021**, *64* (19), 14526−14539.
(18) Zhang, G.; Howe, M.; Aldrich, C. C. Spirocyclic and Bicyclic 8-Nitrobenzothiazinones for Tuberculosis with Improved Physicochemical and Pharmacokinetic Properties. *ACS Med. Chem. Lett.* **2019**, *10* (3), 348−351.
(19) Gao, C.; Ye, T.-H.; Wang, N.-Y.; Zeng, X.-X.; Zhang, L.-D.; Xiong, Y.; You, X.-Y.; Xia, Y.; Xu, Y.; Peng, C.-T.; Zuo, W.-Q.; Wei, Y.; Yu, L.-T. Synthesis and structure−activity relationships evaluation of benzothiazinone derivatives as potential anti-tubercular agents. *Bioorg. Med. Chem. Lett.* **2013**, *23* (17), 4919−4922.
(20) Richter, A.; Narula, G.; Rudolph, I.; Seidel, R. W.; Wagner, C.; Av-Gay, Y.; Imming, P. Efficient Synthesis of Benzothiazinone Analogues with Activity against Intracellular Mycobacterium tuberculosis. *ChemMedChem.* **2022**, *17*, e202100733.
(21) Tiwari, R.; Möllmann, U.; Cho, S.; Franzblau, S. G.; Miller, P. A.; Miller, M. J. Design and Syntheses of Anti-Tuberculosis Agents Inspired by BTZ043 Using a Scaffold Simplification Strategy. *ACS Med. Chem. Lett.* **2014**, *5* (5), 587−591.
(22) Kloss, F.; Krchnak, V.; Krchnakova, A.; Schieferdecker, S.; Dreisbach, J.; Krone, V.; Möllmann, U.; Hoelscher, M.; Miller, M. J. In Vivo Dearomatization of the Potent Antituberculosis Agent BTZ043 via Meisenheimer Complex Formation. *Angew. Chem., Int. Ed.* **2017**, *56* (8), 2187−2191.
(23) Tiwari, R.; Moraski, G. C.; Krchňák, V.; Miller, P. A.; Colon-Martinez, M.; Herrero, E.; Oliver, A. G.; Miller, M. J. Thiolates Chemically Induce Redox Activation of BTZ043 and Related Potent Nitroaromatic Anti-Tuberculosis Agents. *J. Am. Chem. Soc.* **2013**, *135* (9), 3539−3549.
(24) Tiwari, R.; Miller, P. A.; Cho, S.; Franzblau, S. G.; Miller, M. J. Syntheses and Antituberculosis Activity of 1,3-Benzothiazinone Sulfoxide and Sulfone Derived from BTZ043. *ACS Med. Chem. Lett.* **2015**, *6* (2), 128−133.
(25) Eckhardt, T.; Goddard, R.; Lehmann, C.; Richter, A.; Sahile, H. A.; Liu, R.; Tiwari, R.; Oliver, A. G.; Miller, M. J.; Seidel, R. W.; Imming, P. Crystallographic evidence for unintended benzisothiazolinone 1-oxide formation from benzothiazinones through oxidation. *Acta Crystallographica Section C* **2020**, *76* (9), 907−913.
(26) Richter, A.; Goddard, R.; Schlegel, T.; Imming, P.; Seidel, R. W. 2-Chloro-3-nitro-5-(trifluoromethyl)benzoic acid and -benzamide: structural characterization of two precursors for antitubercular benzothiazinones. *Acta Crystallographica Section E* **2021**, *77* (2), 142−147.
(27) Bhakuni, B. S.; Balkrishna, S. J.; Kumar, A.; Kumar, S. An efficient copper mediated synthetic methodology for benzo[d]-isothiazol-3(2H)-ones and related sulfur−nitrogen heterocycles. *Tetrahedron Lett.* **2012**, *53* (11), 1354−1357.
(28) Nishizawa, A.; Takahira, T.; Yasui, K.; Fujimoto, H.; Iwai, T.; Sawamura, M.; Chatani, N.; Tobisu, M. Nickel-Catalyzed Decarboxylation of Aryl Carbamates for Converting Phenols into Aromatic Amines. *J. Am. Chem. Soc.* **2019**, *141* (18), 7261−7265.
(29) Liu, D.; Tian, Z.; Yan, Z.; Wu, L.; Ma, Y.; Wang, Q.; Liu, W.; Zhou, H.; Yang, C. Design, synthesis and evaluation of 1,2-benzisothiazol-3-one derivatives as potent caspase-3 inhibitors. *Biorg. Med. Chem.* **2013**, *21* (11), 2960−2967.
(30) Wu, L.; Lu, M.; Yan, Z.; Tang, X.; Sun, B.; Liu, W.; Zhou, H.; Yang, C. 1,2-Benzisothiazol-3-one derivatives as a novel class of small-molecule caspase-3 inhibitors. *Biorg. Med. Chem.* **2014**, *22* (8), 2416−2426.
(31) Crystal data for **4a**: $C_{14}H_{12.50}F_3N_3O_{4.25}S$, M_r = 379.83, T = 100(2) K, λ = 1.54178 Å, triclinic, space group $P\bar{1}$, a = 10.0915(4), b = 14.5439(5), c = 17.3813(6) Å, β = 78.721(2), γ = 80.711(2)°, V = 2377.82(15) Å^3, Z = 6, ρ_{calc} = 1.592 mg m^{-3}, μ = 2.408 mm^{-1}, $F(000)$ = 1167, crystal size 0.133 × 0.073 × 0.043 mm^3, θ range = 2.69−72.00°, reflections collected/unique = 88503/8735 (R_{int} = 0.0834), 750 parameters, 237 restraints, S = 1.073, R_1 [$I > 2\sigma(I)$] = 0.0420, wR_2 = 0.1499, $\Delta\rho_{max}/\Delta\rho_{min}$ = 0.43/−0.89 e Å^{-3}.
(32) Landge, S.; Mullick, A. B.; Nagalapur, K.; Neres, J.; Subbulakshmi, V.; Murugan, K.; Ghosh, A.; Sadler, C.; Fellows, M. D.; Humnabadkar, V.; Mahadevaswamy, J.; Vachaspati, P.; Sharma, S.; Kaur, P.; Mallya, M.; Rudrapatna, S.; Awasthy, D.; Sambandamurthy, V. K.; Pojer, F.; Cole, S. T.; Balganesh, T. S.; Ugarkar, B. G.; Balasubramanian, V.; Bandodkar, B. S.; Panda, M.; Ramachandran, V. Discovery of benzothiazoles as antimycobacterial agents: Synthesis, structure−activity relationships and binding studies with Mycobacterium tuberculosis decaprenylphosphoryl-β-d-ribose 2′-oxidase. *Bioorg. Med. Chem.* **2015**, *23* (24), 7694−7710.
(33) Liu, R.; Markley, L.; Miller, P. A.; Franzblau, S.; Shetye, G.; Ma, R.; Savková, K.; Mikušová, K.; Lee, B. S.; Pethe, K.; Moraski, G. C.; Miller, M. J. Hydride-induced Meisenheimer complex formation

https://doi.org/10.1021/acsmedchemlett.2c00215
ACS Med. Chem. Lett. 2022, 13, 1302−1310

reflects activity of nitro aromatic anti-tuberculosis compounds. *RSC Medicinal Chemistry* **2021**, *12* (1), 62−72.
(34) Crystal data for **4b**: $C_{17}H_{16}F_3N_3O_6S$, M_r = 447.39, T = 100(2) K, λ = 1.54178 Å, monoclinic, space group $P2_1$, a = 13.4977(4), b = 9.0737(3), c = 15.2780(4) Å, β = 90.489(2)°, V = 1871.09(10) Å^3, Z = 4, ρ_{calc} = 1.588 mg m^{-3}, μ = 2.212 mm^{-1}, $F(000)$ = 920, crystal size 0.161 × 0.062 × 0.051 mm^3, θ range = 2.89−71.99°, reflections collected/unique = 58657/7075 (R_{int} = 0.0634), 600 parameters, 235 restraints, S = 1.099, R_1 [$I > 2\sigma(I)$] = 0.0485, wR_2 = 0.1309, $\Delta\rho_{max}/\Delta\rho_{min}$ = 0.37/−0.29 e Å^{-3}.
(35) Richter, A.; Patzer, M.; Goddard, R.; Lingnau, J. B.; Imming, P.; Seidel, R. W. Structural elucidation of the antitubercular benzothiazinone BTZ043: A combined X-ray, variable temperature NMR and DFT study. *J. Mol. Struct.* **2022**, *1248*, 131419.
(36) Crystal data for **5a**: $C_{14}H_{12}F_3N_3O_4S$, M_r = 375.33, T = 100(2) K, λ = 0.71073 Å, orthorhombic, space group *Pbca*, a = 16.8517(10), b = 7.6877(5), c = 23.4052(14) Å, V = 3032.2(3) Å^3, Z = 8, ρ_{calc} = 1.644 mg m^{-3}, μ = 0.275 mm^{-1}, $F(000)$ = 1538.080, crystal size 0.094 × 0.034 × 0.031 mm^3, θ range = 1.74−31.75°, reflections collected/unique = 96114/5114 (R_{int} = 0.0535), 274 parameters, S = 1.0508, R_1 [$I > 2\sigma(I)$] = 0.0241, wR_2 = 0.0466, $\Delta\rho_{max}/\Delta\rho_{min}$ = 0.46/−0.44 e Å^{-3}.
(37) Crystal data for **5b**: $C_{17}H_{16}F_3N_3O_6S$, M_r = 447.39, T = 100(2) K, λ = 0.71073 Å, monoclinic, space group $P2_1$, a = 7.2884(7), b = 17.5581(16), c = 14.3508(13) Å, β = 98.454(4)°, V = 1816.5(3) Å^3, Z = 4, ρ_{calc} = 1.636 mg m^{-3}, μ = 0.252 mm^{-1}, $F(000)$ = 920, crystal size 0.130 × 0.051 × 0.041 mm^3, θ range = 1.44−48.67°, reflections collected/unique = 434272/34730 (R_{int} = 0.0734), 543 parameters, 1 restraint, S = 1.008, R_1 [$I > 2\sigma(I)$] = 0.0473, wR_2 = 0.1191, $\Delta\rho_{max}/\Delta\rho_{min}$ = 0.57/−0.69 e Å^{-3}.
(38) Kleemiss, F.; Dolomanov, O. V.; Bodensteiner, M.; Peyerimhoff, N.; Midgley, L.; Bourhis, L. J.; Genoni, A.; Malaspina, L. A.; Jayatilaka, D.; Spencer, J. L.; White, F.; Grundkötter-Stock, B.; Steinhauer, S.; Lentz, D.; Puschmann, H.; Grabowsky, S. Accurate crystal structures and chemical properties from NoSpherA2. *Chemical Science* **2021**, *12* (5), 1675−1692.
(39) Neres, J.; Pojer, F.; Molteni, E.; Chiarelli, L. R.; Dhar, N.; Boy-Röttger, S.; Buroni, S.; Fullam, E.; Degiacomi, G.; Lucarelli, A. P.; et al. Structural Basis for Benzothiazinone-Mediated Killing of *Mycobacterium tuberculosis*. *Science Translational Medicine* **2012**, *4* (150), 150ra121.
(40) T, J. A. S.; J, R.; Rajan, A.; Shankar, V. Features of the biochemistry of Mycobacterium smegmatis, as a possible model for Mycobacterium tuberculosis. *Journal of Infection and Public Health* **2020**, *13* (9), 1255−1264.
(41) Lipinski, C. A.; Lombardo, F.; Dominy, B. W.; Feeney, P. J. Experimental and computational approaches to estimate solubility and permeability in drug discovery and development settings1PII of original article: S0169−409X(96)00423−1. The article was originally published in Advanced Drug Delivery Reviews 23 (1997) 3−25.1. *Adv. Drug Delivery Rev.* **2001**, *46* (1), 3−26.
(42) Riccardi, G.; Manina, G.; Pasca, M. R. An effective new drug target for the treatment of tuberculosis. WO2009100731, 2009.
(43) Gopinath, P.; Yadav, R. K.; Shukla, P. K.; Srivastava, K.; Puri, S. K.; Muraleedharan, K. M. Broad spectrum anti-infective properties of benzisothiazolones and the parallels in their anti-bacterial and anti-fungal effects. *Bioorg. Med. Chem. Lett.* **2017**, *27* (5), 1291−1295.
(44) Hoelke, B.; Gieringer, S.; Arlt, M.; Saal, C. Comparison of Nephelometric, UV-Spectroscopic, and HPLC Methods for High-Throughput Determination of Aqueous Drug Solubility in Microtiter Plates. *Anal. Chem.* **2009**, *81* (8), 3165−3172.

https://doi.org/10.1021/acsmedchemlett.2c00215
ACS Med. Chem. Lett. 2022, 13, 1302−1310